TRANSACTIONS OF THE INSTITUTE OF AVIATION
No. 4 (245), pp. 321-337, Warsaw 2016
DOI: 10.5604/05096669.1229486

ISSN 0509-6669
eISSN 2300-5408

CFD ANALYSIS OF AGRICULTURAL AIRCRAFT AERODYNAMIC CHARACTERISTICS

Adam Dziubiński [*], Piotr Jaśkowski [**], Tomasz Seredyn [***]

[*] Centre of New Technologies, Institute of Aviation, Al. Krakowska 110/114, 02-256 Warsaw, Poland,
[**] Design Analysis & Calculation Group, PZL „Warszawa – Okęcie" S.A. Airbus Defence & Space.
[***]Applied Science Faculty, Polish Air Force Academy, Dęblin, Poland
Adam.Dziubinski@ilot.edu.pl, Piotr.Jaskowski@pzl.eads.net, t.seredyn@wsosp.deblin.pl

Abstract

This work is a preliminary part of project concerning the water droplets simulation in agricultural aircraft wake. The CFD results of flow calculation resulting in the aerodynamic characteristics of typical agricultural aircraft, on the example of PZL-106 „*Kruk*", are presented in an operational range of the angle of attack and the sideslip angle. To obtain those characteristics a commercial RANS code was used. The two commonly utilized turbulence models: K-w SST and Spalart-Allmaras are compared in terms of quantitative and qualitative results, especially in range of parameters when a flow separation occurs. The conclusions about range of use for both models are withdrawn. In order to obtain the flight configuration and conditions for final crop dusting simulation, the complete steady aerodynamic properties of the aircraft have been calculated, described and are available for other studies. Where available, the characteristics are compared with the experimental results. The results are also provided in form of distribution on the predefined aircraft parts, which is hard to obtain with the use of wind tunnel tests.
Keywords: CFD, agricultural aircraft, turbulence model.

1. INTRODUCTION

The aircraft, which is the subject of this work, has a rather low operational speed and flight velocity, in a range of 170-180 km/h (91 - 97 kts) [1, 2], so it does not have refined aerodynamics in terms of drag reduction. The shape of the airframe includes such elements as: landing gear, wing and horizontal stabilizer struts and all external agricultural equipment which is also a huge drag generator. On the other hand, this aircraft has rather sophisticated lifting surface equipped with high lift devices, slats and slotted flaps allowing to use it in the slow, low level flight in a ground proximity during crop dusting. One of the main features of good agricultural aircraft is its ability to fly low and slowly to avoid the dispersion of sprayed medium on the area other than specified. The medium usually consists of the compounds of high toxicity, at least at the time of appliance, since all the pesticides, herbicides and fungicides have its grace period, after which it has to dissolve into the non-toxic compounds. Consequently, the medium has to be applied to the field in a possible uniform and even way, which should not be introduced into the pilots' cabin and have a minimal contact with the external surface of the fuselage. The CFD methods, as used in this work, are a good tool to predict those

characteristics. Since the analyses of spraying process are made in a steady flight, the conditions of level flight has to be obtained and this process is described in this paper. The aircraft, which is the subject of this work, i.e. a PZL-106 „*Turbo Kruk*" (Fig. 1), is a 2-seat, specialized agricultural design. Originally designed in the early '70s [3], the aircraft came through a huge metamorphosis when the radial engine was replaced by a more advanced, yet lightweight, turboprop engine, which extended its nose [2].

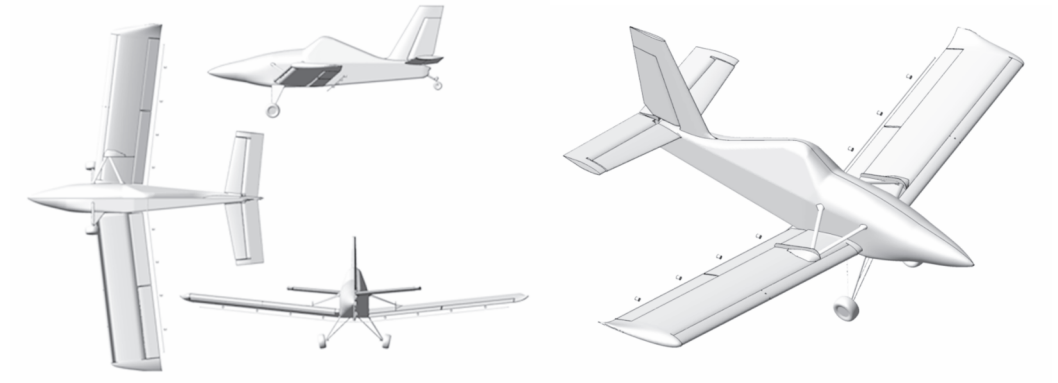

Fig. 1. Three views (left) and isometric view (right) of PZL-106 „*Turbo Kruk*" aircraft geometry [Dziubiński, 2016]

The PZL-106 has a design which is now common to all crop-duster aircraft where the tank for chemicals is placed between the cockpit and the engine and fuel tanks are mounted inside the wings. This design is defined by its crash worthiness. When this slow-flying aircraft crashes, the engine and tank shield the pilot and amortize the crew cabin. The wings during such a crash usually break and move forward, so even if a fuel tank leak appears, it is far from hot parts of the engine. Usually, the engine is already covered with the chemicals which mainly consists of water. This aircraft is also well known for its cabin crash worthiness where all the struts are designed to bend outwards in the case of a flip over. The geometry of PZL-106 is based on the original factory CAD drawings [4].

2. RESEARCH METHOD

The conditions of level flight in terms of the angle of attack are different for specific country (terrain height above the sea level, air temperature). It depends on flight time (an aircraft uses its fuel, the chemicals are also sprayed out) and the height over the ground (so-called „ground proximity effect"). In order to predict the aircraft characteristics the whole operational range of the angle of attack has to be tested. Also, some simplifications have to be assumed in order to avoid a multiplication of the calculation cases amount. It was assumed as follows:

– all the simulations are made in Standard ISA conditions at the sea level,
– the ground influence is neglected at that point,
– the influence of the propeller wake and swirl has been ommitted,
– all control surfaces are fixed in null deflections.

The flow simulations are computed with the use of Reynolds Averaged Navier Stokes (RANS) equation solver based on finite volumes method. A commercial code – ANSYS Fluent – is chosen for this purpose [5]. The main set of governing equations is closed with Spalart-Allmaras turbulence model equation, known as standard in external flow simulations but assuming a turbulent flow [6,7]. Another set of simulations is made using Menter K-w SST 4-equation turbulence model, more

adequate in terms of the flow turbulization prediction [8-10]. Since the PRESSURE FARFIELD condition was used on fluid boundary of the domain, the ideal gas model of density, as demanded by this condition, is also assumed.

The CFD method has this feature, contrary to the experimental and the wind tunnel methods, by means of which obtaining information on the forces acting on an isolated part of a model is definitely easier. It is a good tool to understand the influence of selected parts on any specified quantity or aerodynamic characteristics. In order to obtain such information, a model is divided into separate parts, as shown in Fig. 2. All the zones represent the WALL boundary condition, except the FAN zone which is used in the simulation as a simplification of the propeller. To obtain information on the propeller wake influence, a condition with a similar name – FAN – is set on this surface. The actuator disc model could be used here to simulate the propeller with constant pressure jump. This model is adequate to obtain flow velocity increase due to the propeller action, but it is not sufficient to depict the wake swirl. Since this information about the original propeller is unknown, such a simplification is also reasonable. The following simulations are made with a null pressure jump, because this propeller model will be used in further spray simulations at a steady flight condition, when the drag of airframe will be known, and the propeller thrust could be set.

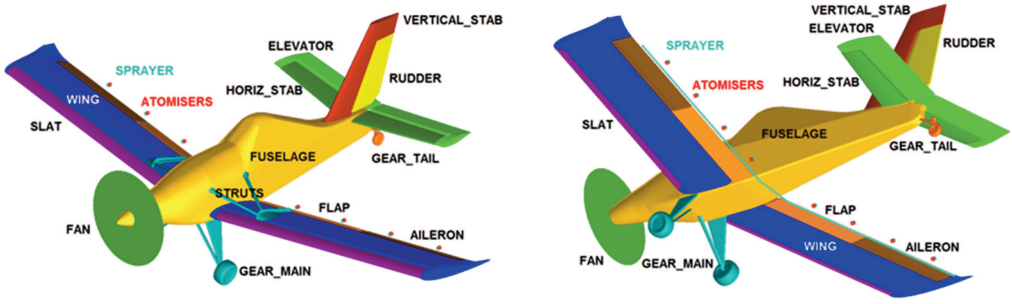

Fig 2. Division of airframe surface into zones including FAN double-sided surface zone for pressure-jump simulation of propeller influence [Dziubiński, 2016]

At the external fluid surfaces of the domain, a PRESSURE FAR FIELD condition was set. At the back wall of the domain a PRESSURE OUTLET boundary is used, due to the fact that when in the domain a source of momentum appears (and usually a FAN condition is treated as one), the solution converges better when a disturbed flow exits with outlet than with a far field. This is particularly important in the calculations concerning helicopters and propeller driven aircraft.

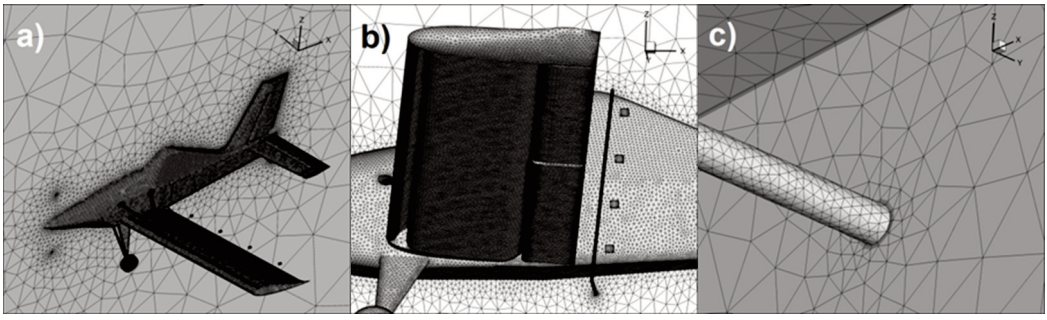

Fig. 3. Mesh density on the model of an aircraft (a) and details of its shape (b), including a model of boundary layer near walls of the airframe geometry (c) [Dziubiński, 2016]

The computational mesh, size of $3.2*10^6$ elements (cells), is a tetrahedral non-structural mesh with prismatic elements of the boundary layer. This kind of mesh is usually better to generate around the models with complicated geometry, and such aircraft with all struts, sprayer, non retracting landing gear, slats and slotted flaps, could be easily treated as one. The Y+ turbulence parameter of this mesh is assumed to be in the range of: Y+=<30-200>, which is suggested for both of the used turbulence models: Spalart-Allmaras and Menter K-w SST. Details of the mesh and density of the elements are shown in Fig. 3. The low density of a mesh on propeller could be a matter of discussion, but since only the pressure is not constant along the flow through the propeller disc and other flow parameters, such as the velocity field, are not changing rapidly, this density of the mesh is sufficient.

It is a good practice in CFD to make calculations in a design coordinate system (or at least have a mesh in this coordinate system) but to extract the forces and moments in flow coordinate system, as it is done in wind tunnels. That way the quantities could be probed in exact places of the model, as the designer requires, but the aerodynamic characteristics are comparable to the experimental ones. This is the reason for using the two coordinate systems in this work (Fig. 4): a design one (given in CAD geometry) $OX_OY_OZ_O$, with the center at the firewall of the engine and an aerodynamic one, AXYZ, with the center in the design center of gravity, usually placed at the 1/4 of mean aerodynamic chord projection on symmetry surface and rotated by the actual angle of attack and the sideslip angle.

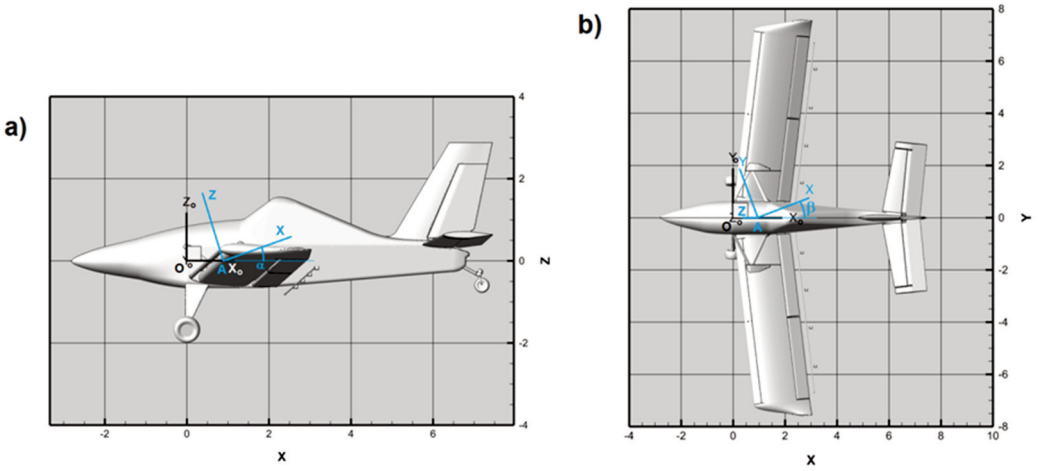

Fig. 4. Coordinate system used in this work and positive values of angle of attack (a) and sideslip angle (b) [Dziubiński, 2016]

Force coefficient components are defined as follows:

$$Cx = \frac{Px}{\frac{1}{2}\rho V^2 S}; Cy = \frac{Py}{\frac{1}{2}\rho V^2 S}; Cz = \frac{Pz}{\frac{1}{2}\rho V^2 S} \tag{1}$$

Where: $\vec{F} = (Px, Py, Pz)$ – the aerodynamic force, r – the air density, V – the airspeed, S – the wing surface including the part submerged in the fuselage. All the moment coefficient components are related to the wing mean aerodynamic chord:

$$Cmx = \frac{L}{\frac{1}{2}\rho V^2 Sc}; Cmy = \frac{M}{\frac{1}{2}pV^2 Sc}; Cmz = \frac{N}{\frac{1}{2}\rho V^2 Sc} \tag{2}$$

Where: $\vec{M} = (L, M, N)$ – the aerodynamic moment, c – the Mean Aerodynamic Chord (MAC) of the wing.

3. RESULTS

The following part of this work is divided into two chapters: the analysis of the angle of attack and the angle of sideslip influence on the aerodynamic characteristics. For both of them, the qualitative and quantitative results are shown. The comparison between turbulence models is made only for the angle of attack, since there is a difference in a separation process that can be observed.

3.1. Angle of attack

The qualitative results comparison between the Menter K-w SST and the Spalart-Allmaras (S-A) turbulence models (Fig. 5. left) shows very good overall agreement in drag, pitching moment and linear part of lift coefficient values. The main difference appears in the stall area where the S-A shows a delay in detachment which leads to a higher maximum lift value. The stall is more benign in the SST model (the lift curve is less pointy upwards), but both models predict rather mild characteristics of stall, which is a good feature for an aircraft flying low and slowly near the ground.

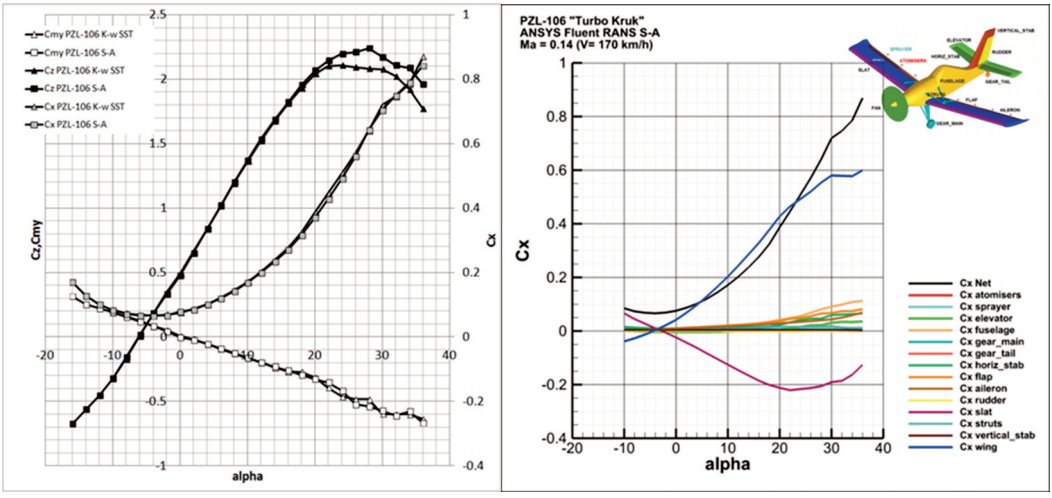

Fig. 5. Aerodynamic characteristics of PZL-106 aircraft: comparison between two turbulence models (left) and distribution of drag coefficient between airframe components (right) [Dziubiński, 2016]

The distribution of drag coefficient components on zones (Fig. 5. right) shows that the main influence on this parameter has a wing and a slat and when the influence on drag from the wing increases, the influence of the slat decreases down to negative values. The fuselage influence on drag appears at high angles of attack. The negative values of drag for the slat, meaning that this part of the wing pulls the aircraft forward, is a result of close interference between the slat and the main wing. Because of that, the wings usually have a tendency to break forward in stall because the underpressure peak acting on the upper front surface of the wing is directed slightly forward. The same force component propels the helicopter rotor during autorotation. The drag characteristics are usually shown for net sum of all zones rather than its particular values and it is clearly visible that the sum of all the drag components is always positive.

When analyzing the lift coefficient distribution along the airframe components (Fig. 6, right), again, the wing and the slat become the main contributors. The stall begins at the wing first and it is not visible further in wall shear/pathlines maps. This is due to the fact that usually the stall on multi element airfoil appears between the layers of flow. The bottom layer (under the separation) attaches to the wall even if it was not attached before stall. The observation of a surface flow could be misleading and the separation begins on the main wing, not on the slat.

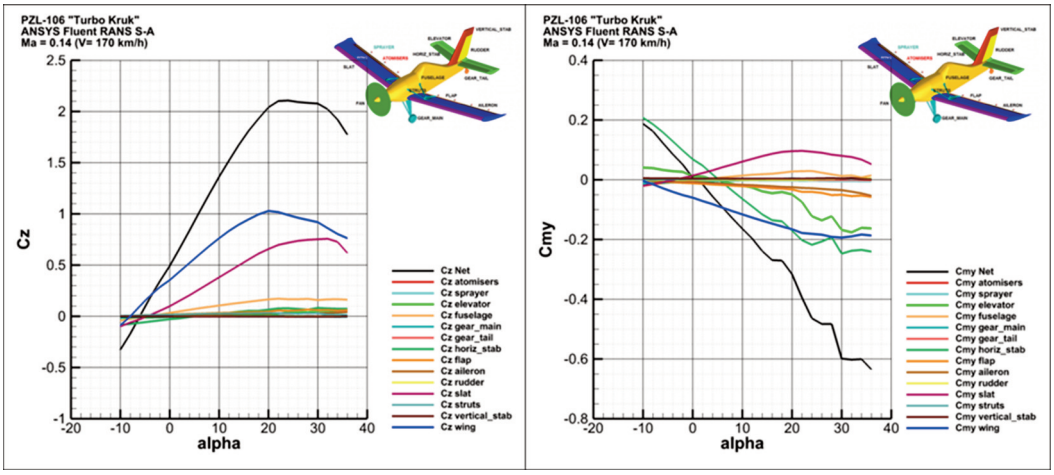

Fig 6. Distribution of lift coefficient (left) and pitching moment coefficient (right) between airframe components. [Dziubiński, 2016]

Considering the moment coefficient distribution on zones, it is clearly visible which parts work for and which ones work against the aircraft longitudal stability. The main de-stabilizers are the slats but also the fuselage on the high angle of attack. The main stabilizers are the wing and the horizontal stabilizer coupled with the elevator. There is a slight stabilizing influence of the flap and the aileron but all the other parts have a neutral influence.

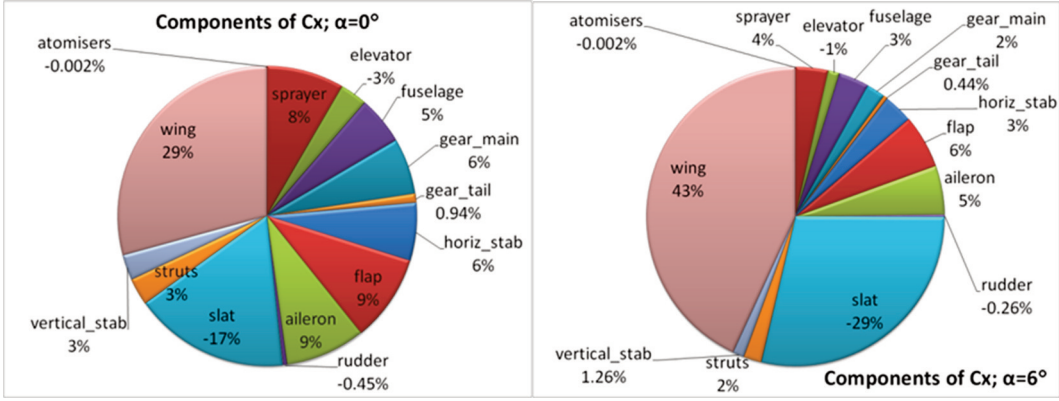

Fig. 7. Percentage of PZL-106's drag components for two selected angles of attack [Dziubiński, 2016]

In order to extend the information about the distribution of drag components, which is the most important for the designers when analyzing the performance of an aircraft, it is shown in the form of pie-chart for two chosen angles of attack (Fig. 7). It allows getting to know the percentage of drag caused also by the smaller sources. Surprisingly, the main landing gear has only 6% share of the total

drag at α=0º and 2% at α=6º respectively, also the struts (3% at α=0º) and the tail gear (1% on both shown angles) have a minimal drag influence. At this background, the sprayer with its 8% at α=0º and 4% at α=6º is a relatively high source of drag. In Fig. 8 such a device is shown, compared with a geometry representation in the following work. The difference in the position of rake below the wing trailing edge is caused by the fact that the geometry was based on factory technical drawings and the picture depicts the owner's field modification of sprayer equipped with the atomizers. In Fig. 9 a central pump equipped sprayer is shown, which (the pump) is omitted in geometry, because the lack of the documentation. This device should further increase the aircraft drag.

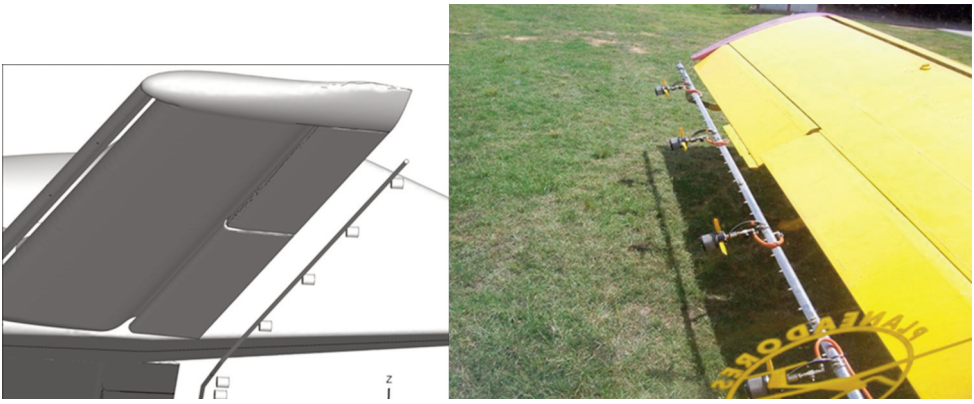

Fig. 8. The simplified geometry of sprayer, with the additional atomizers mounted on the rack of nozzles (right) and a similar design of the PZL-106 field modification [Dziubiński, 2016] [13]

Fig. 9. The aircraft equipped with a similar sprayer to the one used in this work with the central pump propelled by an external flow axial turbine, omitted in the computational geometry [13]

In Fig. 10 and 11 the flow detachment at the positive and negative angles of attack are shown respectively. At the positive angle of attack the separation begins on horizontal tail at the angle of attack α=16º starting from the root section of the elevator. The results of separation appears to be visible at the slat area near the struts mounting point and on the main wing between the fuselage and struts mounting point, at the angle of attack α=20º. The separation on the upper side of the wing does not change up to α=30º, when on the area near the struts mounting point the air re-attaches and the separation appears along the anti-stall fence.

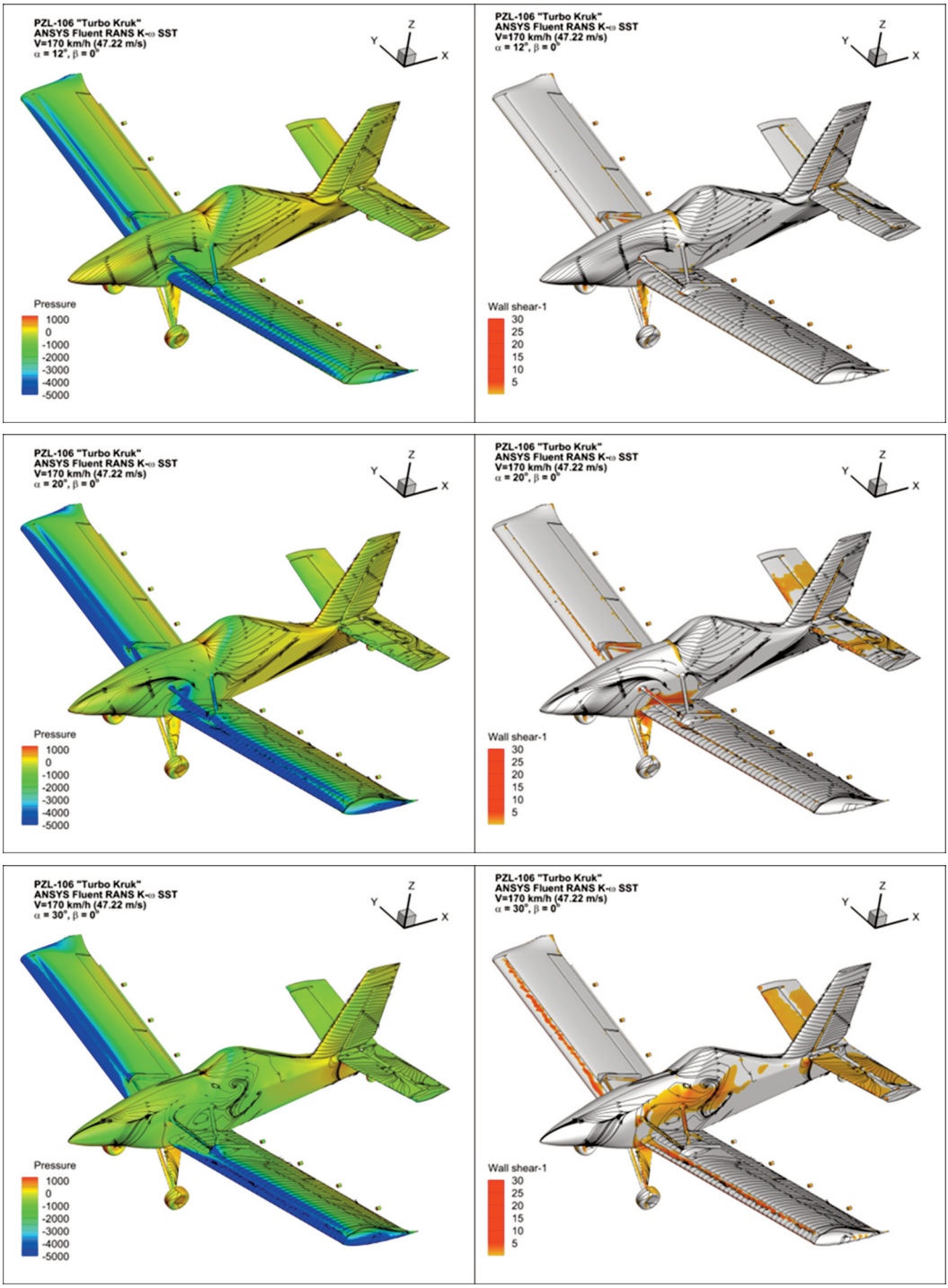

Fig. 10. Pressure distribution (left) and flow detachment areas (right) completed with pathlines for separation at positive angles of attack [Dziubiński, 2016]

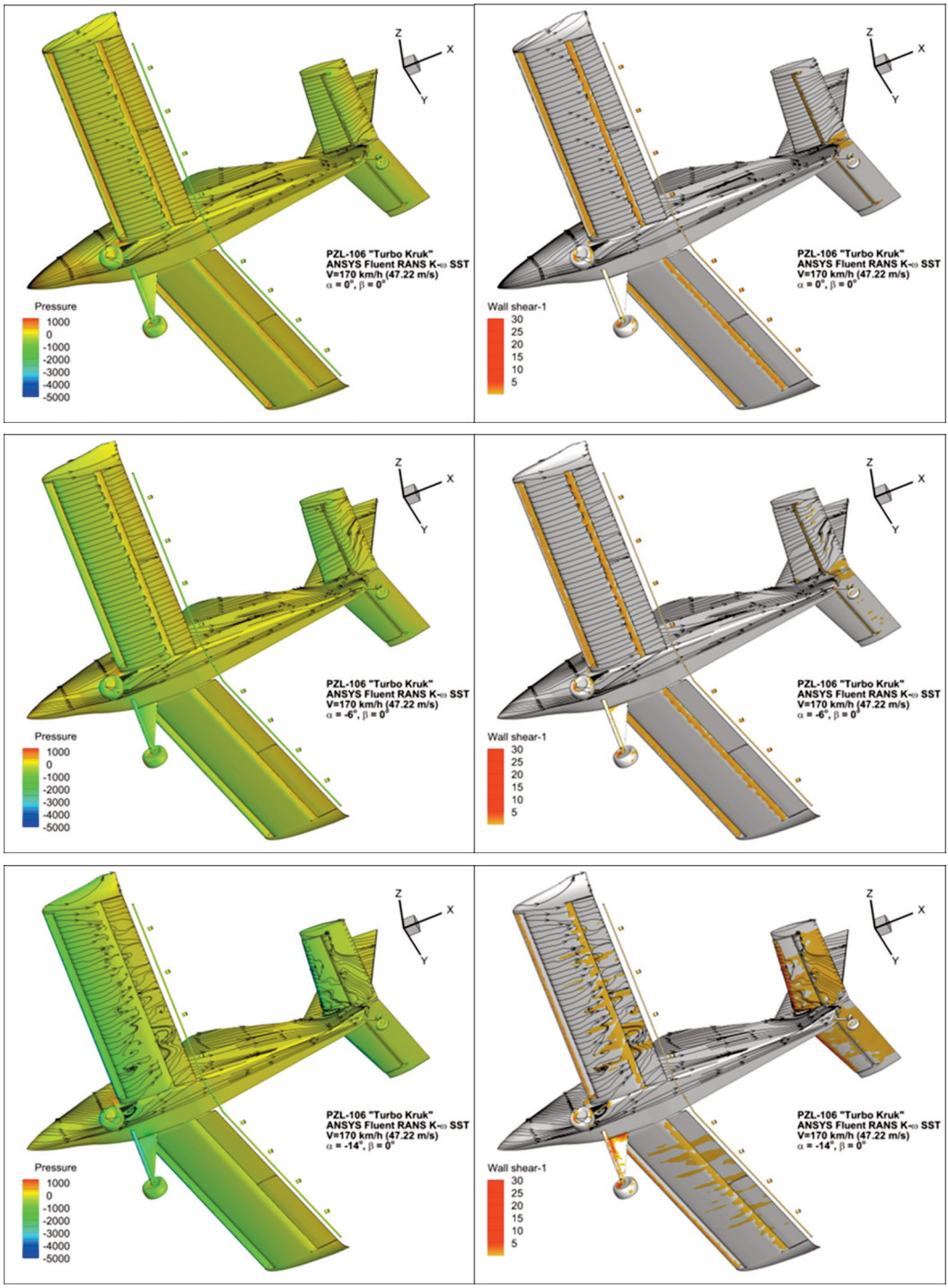

Fig. 11. Pressure distribution (left) and flow detachment areas (right) completed with pathlines for separation at negative angles of attack [Dziubiński, 2016]

At the negative angles of attack (shown in Fig. 11) the stall of horizontal surface appears at α=-6º on the whole length of the elevator. The separation on the main wing appears at α=-14º also on the whole area of the flap and the aileron and on the main wing near the struts mounting point, which is interesting since the struts are mounted on the opposite side of the wing and the main landing gear is too short to have any influence. The separation on the wing equipped with constant slat and slatted flaps is interesting, since it is a well-known fact that while turning back during a gaining altitude maneuver or after a sudden drop of a water bomb, an aircraft often unintentionally is put into an inverse flight, which leads to an uncontrolled spin near the ground, as in [11]. The aircraft like PZL-106 „*Kruk*" and PZL M-18 „*Dromader*" do not have such a tendency, even when the slats and flaps are a factor which should make that inclination worse.

3.2. Sideslip angle

Often an aircraft flies in a crosswind condition, and in order to keep its position over the field, it has to fly with some non zero sideslip angle. The authors found it necessary to obtain the sideslip aerodynamic characteristics of an example aircraft. The range of calculations was chosen to be β = <0º,26º> and within this range a stall of the tail vertical surface was observed. This range is an operational one and the aircraft is treated as a symmetrical one. In terms of aerodynamic characteristics it is so, but since the engine has some angle of inclination, when analyzing the influence of the propeller, this simplification is inadequate.

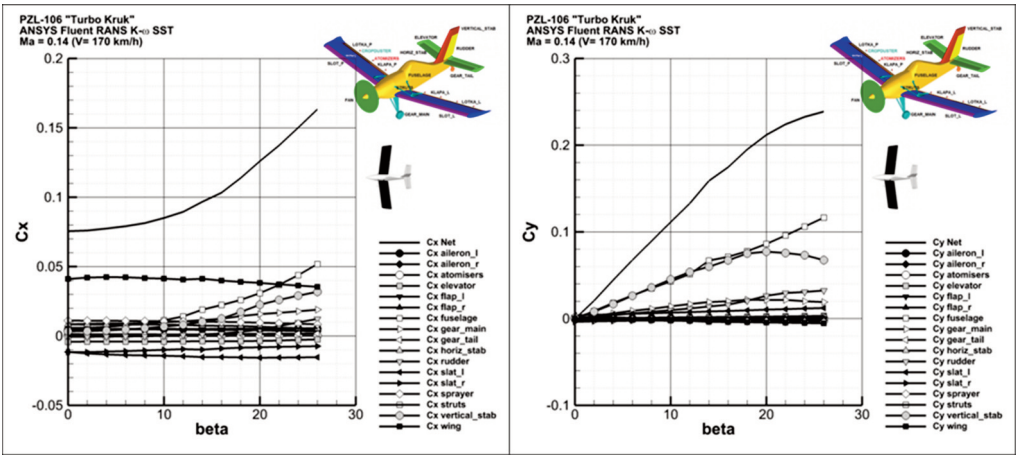

Fig. 12. Distribution of the drag and the side force coefficients between airframe components with increase of the sideslip angle. [Dziubiński, 2016]

All six components of the external force and moment are presented in Fig 12-14. The main drag component is generated by the wing (Fig. 12 left). With the increase of sideslip angle, the influence of fuselage, vertical stabilizer and the main landing gear increases. The negative (as it was mentioned above) drag component of slats shows that for this slightly skewed wing the difference is as follows: the left (forewind) slats drag decreases (its absolute value increases) and the right one increases. This shows that for upwind wing the slat works better, because it is not shadowed aerodynamically and less influenced by the upstream sideslip than the other one. The increase/decrease tendency is adequate for both slats, so the first one gains drag as much as the other one loses it. It leads to the conclusion that rather a skewness is a factor than the aerodynamic shadow. Side force coefficient (Fig. 12 right), one of the two main components (with yaw moment) tested in this part, has two main contributors, for which the influence is surprisingly similar: the fuselage and the vertical stabilizer.

The rudder influence is much lower, and it has a similar size to the main gear influence. Starting from β=18º a flow detachment appears on the rudder and the vertical stabilizer and has a form of a mild, very slow stall. This is the proof of a good directional stability and an easy yaw recovery for this aircraft.

The main contributor of the lift (Fig. 13 left) is a wing, slight positive lift is generated by the slats and slight negative by the horizontal tail surface. The positive influence of the fuselage on the lift is interesting and it increases with the sideslip angle in a parabolic way, up to 20% of the whole lift at β=26º.

For a roll moment (Fig. 13 right) almost all components pull the aircraft to rise the forewind wing and to turn sideways to the wind. Only the right (forewind) slat works against this tendency, but its action is balanced by the left one. Their influence does not change much with the sideslip angle, as it happens for the vertical stabilizer and the wing (it is one part, not divided into the left and right one), for which the influence is mostly linear because the stabilizer also shows the stall influence.

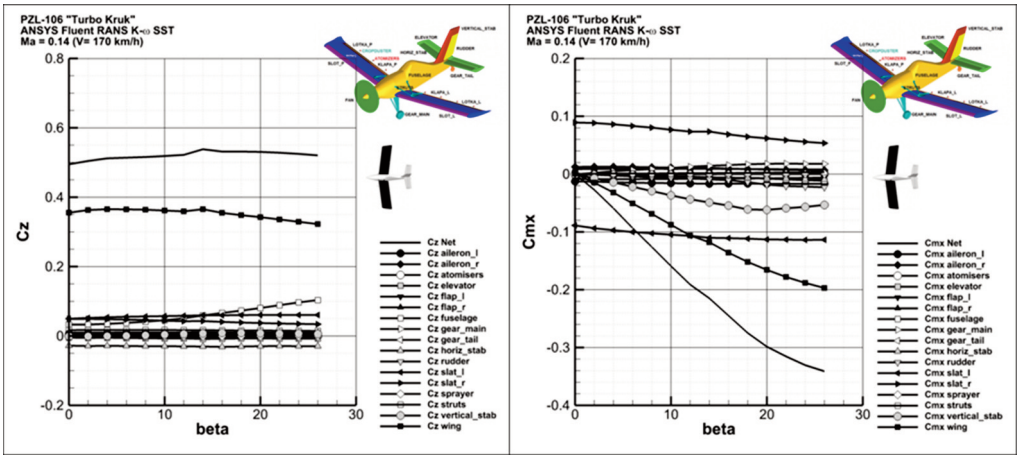

Fig. 13. Distribution of the lift force and the rolling moment between airframe components with increase of the sideslip angle. [Dziubiński, 2016]

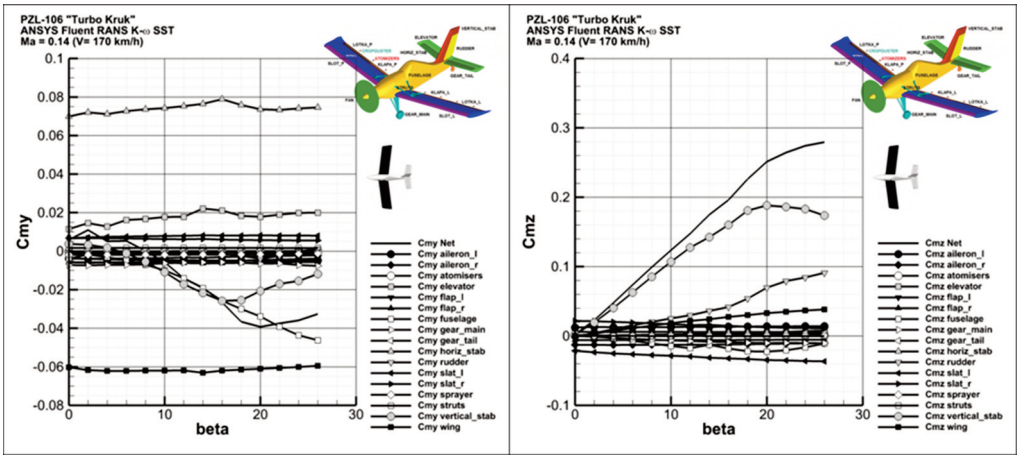

Fig. 14. Distribution between airframe components shares of the pitching and the yawing moment with increase of the sideslip angle. [Dziubiński, 2016]

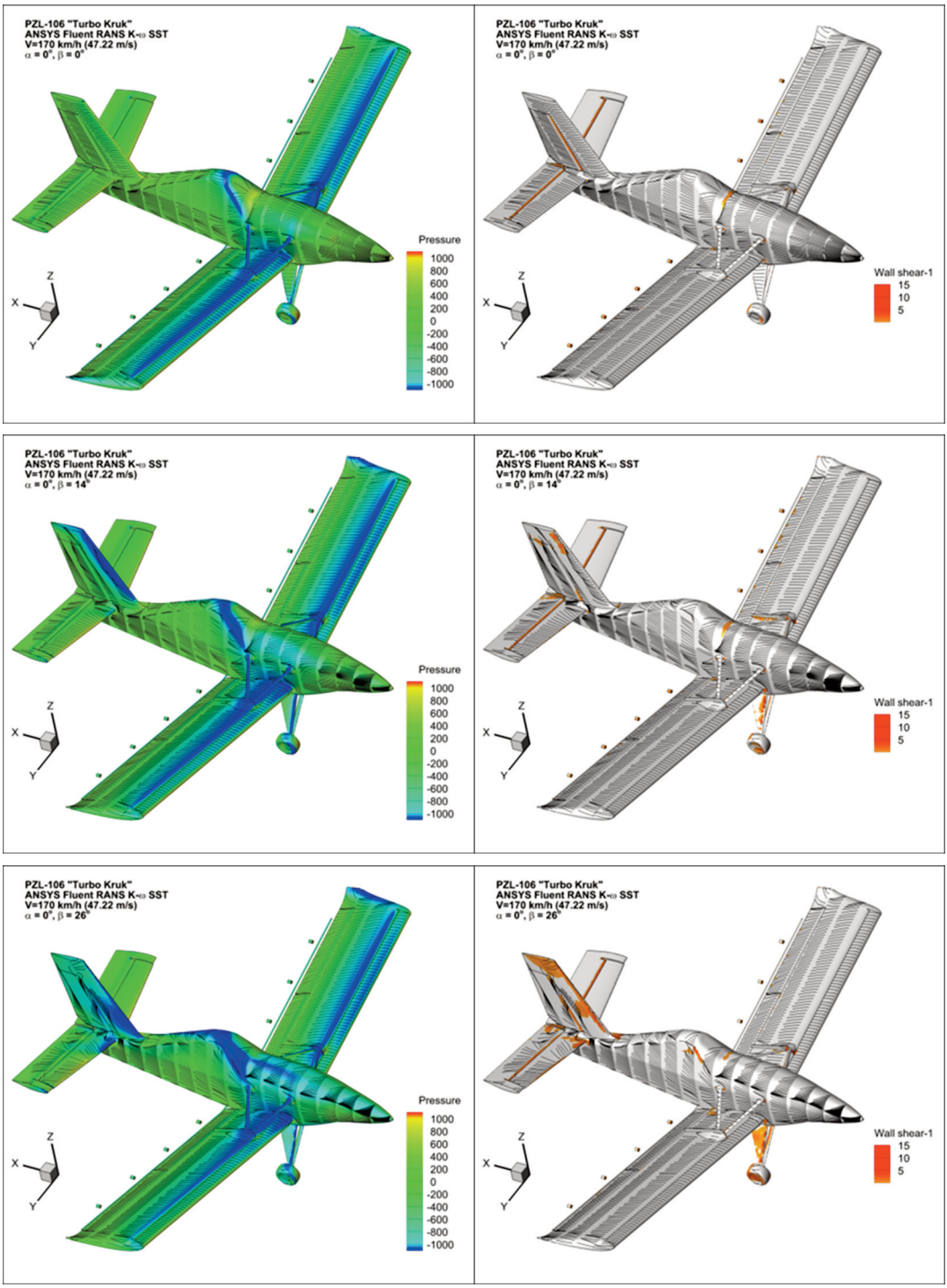

Fig. 15. Pressure distribution (top) and flow detachment areas (bottom) completed with the pathlines for separation development at positive angle of sideslip [Dziubiński, 2016]

Pitch moment characteristics are rather constant for its main contributors - the wing and the horizontal stabilizer (Fig. 14. left). There is some visible influence of the elevator, which could be treated as constant. But, since their actions are similar, the factor in the pitch moment change becomes a pitch influence of fuselage (linear above β=10º) and vertical stabilizer, for which the stall influence is very nonlinear. As a result, the aircraft in the crosswind flight has a negative pitching moment character and a nose-down tendency.

Yawing moment, which is the other main factor in this part of calculations (Fig. 14 right) has one main contributor, i.e. the vertical stabilizer. The influence of the rudder is also visible, but rather at a high angle of attack. The influence of the fuselage is rather low taking into account its long nose, which usually destabilizes the aircraft. Its influence (negative yawing moment) is lower than a negative influence of the left slat.

The quantitative analysis of flow with sideslip angle (Fig. 15) shows, that at β=14º the flow on backwind (suction) surface of the tail stabilizer is turning to cross flow directed to the tip. Since it is a surface with a high skew angle, the flow shortly becomes separated but, as it could be interpreted from a pressure map, a vortex flow appears, which makes the separation smooth and increases the tail effectiveness at high angle of sideslip. At β=14º also a separation on the main landing gear appears. The separation does not appear on the backwind side of the fuselage up to β=26º except small separation bubbles near the canopy windshield and doors.

4. DISCUSSION

The results obtained with the CFD method, using Reynolds Averaged Navier Stokes solution with the finite volumes method, coupled with an advanced Menter K-w-SST, showed that the aircraft has a wide range of operational angle of attack and sideslip angle. The proper modeling of high lift surfaces, slotted flaps and slats, but also the gaps between the stabilizer and the rudder, results in prediction of characteristics which are adequate to those of the existing aircraft. This method also allows to obtain the influence of parts like the landing gear, wing struts and the sprayer on drag of the aircraft, which was hard to predict using panel methods [12], and the experimentally obtained values had to be used. Now, the same values can be obtained in a real scale of the model and flow, contrary to the wind tunnel, where both conflict of Mach vs. Reynolds number and size difference take their part of error.

An error of the numerical solution, both discretisation and modeling, is also a factor and in order to avoid it a proper procedure of the mesh sizes setting, boundary conditions and governing equations had to be assumed. But still the two main topics have to be discussed in this part: the influence of the turbulence model used in the simulations and the accuracy of the results as compared with available results for this type of aircraft.

4.1. Difference in stall prediction between K-w SST and S-A

The difference between Menter and Spalart-Allmaras turbulence models have been discussed partially during the angle of attack analysis, but here the reason, which caused the difference in the maximum lift coefficient and the character of stall is still to be shown. The Menter model has been used in many works [8-10] and is treated usually as more accurate than the Spalart-Allmaras, since it better resolves the boundary layer behavior in terms of turbulization, detachment and re-attachment of flow.

Menter K-w SST 4-equation model

Spalart-Allmaras 1-equation model.

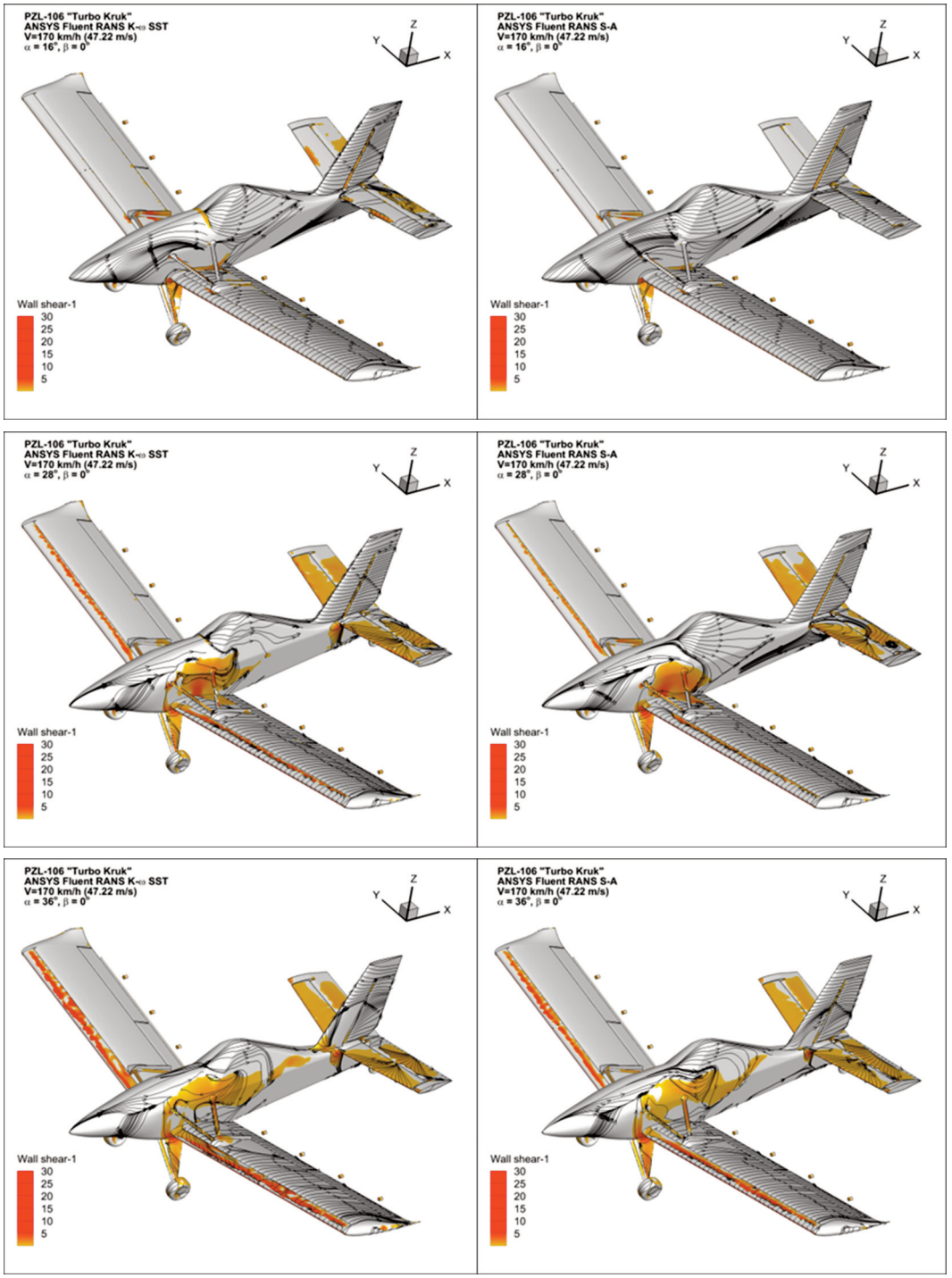

Fig. 16. Difference in prediction of flow detachment areas between the Menter K-w SST(left) and the Spalart-Allmaras (right) turbulence models [Dziubiński, 2016]

The main differences in flow detachment could be explained using Fig. 16. The Menter model predicts the flow detachment on the elevator at a lower angle of attack than the Spalart-Allmaras, namely at α=16º, but even then, the tip of the stabilizer is still in attached flow. The separation on the main wing appears at α=28º on the slat and in the area between the stall fence and the fuselage in both cases, but the separation on the slat is present on a greater area in K-w SST, also in the root part of it. In a deep stall conditions both models show separation on the elevator and the slat, reattachment in the area between stall fence and the fuselage, a wake shadow on the fuselage and root of the vertical stabilizer, but in the S-A model the separation is less intensive, does not cover the whole slat and, probably for that reason, the higher values of lift coefficient are obtained.
The K-w SST model better describes the maximum forces acting on the airframe structure, and those results should be used in load calculation. The Spalart-Allmaras model predicts lower maximum lift, and its prediction is on the safe side when this design feature is taken into account.

4.2. Agreement between calculations and available experimental results

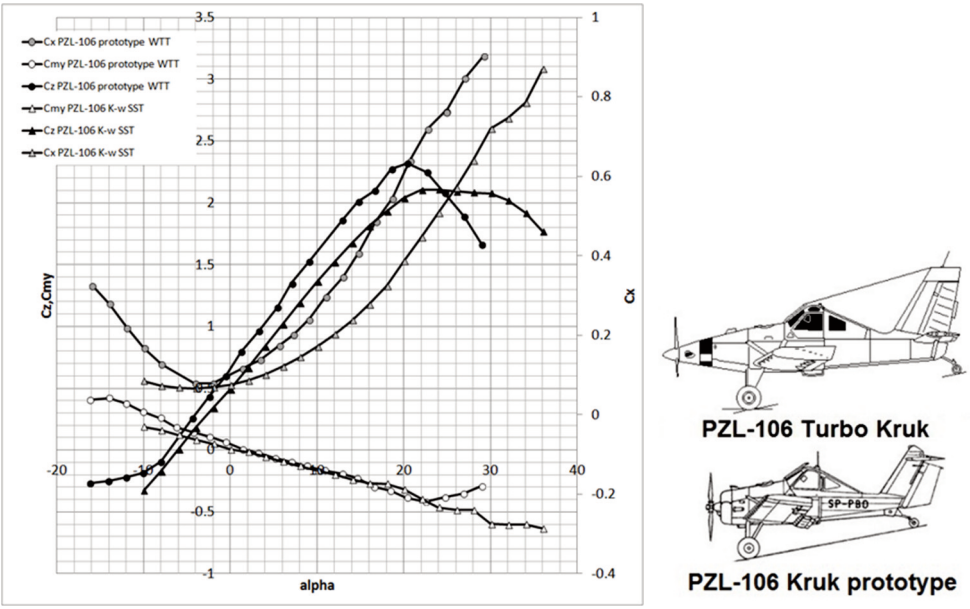

Fig. 17. Comparison between wind tunnel results of „Kruk"prototype [14] and CFD results for „Turbo Kruk" [Dziubiński, 2016][3]

The comparison of results between the wind tunnel [14] and the calculations (fig. 17) has been made to test if the calculation results are valid. The differences between those two models are as follows: the wind tunnel model has a radial piston engine, tail horizontal surface on top of the vertical stabilizer, but most importantly, it has a different airfoil on the wing - a *Clark Y*. The turbine version of „Kruk" has an *NACA 2415* airfoil. Of course, during the change of airfoil, a redesign of gaps between the flap, the aileron, the slat and the main wing has been done and that is shown in lift characteristics. The difference between drag characteristics is a response mainly to the change of the engine. Despite this, a real proof of the calculation validity is the fact that there is a good correspondence between moment characteristics, which is mainly an influence of the horizontal stabilizer surface, and this, except its position, has not changed. The correspondence between wind tunnel tests and calculations is weak (except the pitching moment), but all the differences are easy

to explain and do not deny the validity of calculations. Unfortunately, both the flight test data and the wind tunnel test results for the Turbo version are unavailable, so one of the future steps of this research should be to obtain those experimental data. Also, having the data the discussion about accuracy of turbulence model could be better reasoned. The other way is to recreate the prototype geometry and compare those calculation results with WTT, which is also a proposed further direction of the study.

5. CONCLUSIONS

In the work a possibly complete aerodynamic characteristics of a PZL-106 „*Turbo Kruk*" have been obtained numerically, both against the angle of attack and the sideslip angle. The value of this work lies in the presentation of results also as the distribution between the airframe parts its share of all components of aerodynamic force and moment for both analyzed factors: angle of attack and sideslip angle. Additionally, two models of turbulence have been compared in terms of qualitative and quantitative results. The symmetric analysis results have been compared to available wind tunnel test results and despite the differences, which could be reasonably explained, proved to be corresponding to the experiment. Ambition of the authors was to provide the designers with complete information about the aircraft aerodynamics. The results are planned to be used for further analyses of flow behind the aircraft as the input flow condition in spray system analysis and water droplets simulations. An analysis of the turbulence models led to two conclusions. First, the K-w SST model better describes the maximum forces acting on the airframe structure, and those results should be used in a load calculation. The second conclusion is that the Spalart-Allmaras model predicts lower maximum lift, and its prediction is on the safe side when this design feature is taken into account.

BIBLIOGRAPHY

[1] W. K., 1981, „PZL-106A Kruk", Technika Lotnicza i Astronautyczna, 5/81, Wydawnictwa Komunikacji i Łączności, Warsaw, pp. 15-16.

[2] „PZL-106BT-601 Turbo Kruk", Technika Lotnicza i Astronautyczna, 4-5/86, Wydawnictwa Komunikacji i Łączności, Warsaw, pp. 14-16.

[3] Glass A. et al., 2004, „Problemy rozwoju samolotu PZL-106 Kruk", Polska Technika Lotnicza – Materiały Historyczne (4/2004), from http://www.smil.org.pl/ptl/wyklady/04_PZL-106_Kruk.pdf

[4] PZL Warszawa Okęcie S. A., 2014, CAD Geometry of „Turbo Kruk", Warsaw.

[5] ANSYS, „ANSYS Fluent 14.5 User's guide".

[6] Dziubiński, A., Stalewski, W. and Żółtak, J., 2008, „Przykłady zastosowania pakietu Fluent ™ w analizach bezpieczeństwa lotu śmigłowców", Prace Instytutu Lotnictwa, 194-195, pp. 146-157.

[7] Łusiak, T., Dziubiński, A. and Szumański, K., 2009, "Interference between helicopter and its surroundings, experimental and numerical analysis", TASK Quarterly, 13(4), pp. 379-392.

[8] Sobczak, K., 2008, „Modelowanie wybranych przvpadków lotu śmigłowca z wykorzvstaniem oprogramowania FLUENT"., Prace Instytutu Lotnictwa, 194-195, pp. 158-165.

[9] Szafran, K., Shcherbonos, O. and Ejmocki, D., 2014, "Effect of duct shape on ducted propeller thrust performance", Transactions of the Institute of Aviation. 4(237), pp. 85-91.

[10] Sieradzki, A., Dziubiński A. and Galiński C., 2016, „Performance Comparison of the Optimized Inverted Joined Wing Airplane Concept and Classical Configuration Airplanes", Archive of Mechanical Engineering, 63(3), pp. 455-470.

[11] „Air Tractor Inc AT-802, VH-ODL", Aviation safety investigations & reports, Australian Transport Safety Board„ from https://www.atsb.gov.au/publications/investigation_reports/1998/aair/aair199800640

[12] Błaszczyk P., Goetzendorf-Grabowski T., Goraj Z., and Sznajder J., 1998, „Modeling of Unsteady Flow about a Fire Fighting Aircraft Dropping the Water Bomb", 36th AIAA Aerospace Sciences Meeting and Exhibit. Reno, NV, U.S.A
[13] photo courtesy of PZL Warszawa - Okęcie.
[14] Kacprzyk, J., 1974 „Badania aerodynamiczne modelu samolotu PZL-106-U04-SK", report of IoA no. 27/PR/74, Warsaw.

ANALIZA NUMERYCZNA WŁASNOŚCI AERODYNAMICZNYCH SAMOLOTU ROLNICZEGO

Streszczenie

Praca stanowi część prac przygotowawczych do analiz ruchu kropel wody w zaburzeniu za samolotem rolniczym w trakcie oprysku. Zamieszczono tu rezultaty symulacji numerycznych opływu wokół typowego samolotu rolniczego. Używając jako przykładu samolotu PZL-106 „*Kruk*" otrzymano charakterystyki aerodynamiczne w funkcji kąta natarcia i kąta ślizgu dla użytkowych zakresów tych parametrów. Do obliczeń użyto komercyjnego kodu z zakresu obliczeniowej mechaniki płynów, który rozwiązywał równania Naviera - Stokesa metodą uśrednień Reynoldsa (RANS), wykorzystując przy tym dwa modele turbulencji: K-w SST oraz Spalart-Allmaras. W pracy porównano oba te modele i przedstawiono wnioski co do zakresu ich zastosowania. W celu uzyskania prawidłowej konfiguracji przelotowej w trakcie oprysku otrzymano drogą obliczeniową kompletne statyczne charakterystyki aerodynamiczne badanego samolotu. Gdzie było to możliwe, porównano je z posiadanymi wynikami eksperymentalnymi. Wyniki te są przedstawione również w postaci udziałów poszczególnych elementów płatowca, które trudno byłoby uzyskać na drodze eksperymentu tunelowego.
Słowa kluczowe: aerodynamika numeryczna, samolot rolniczy, model turbulencji.

Acknowledgement

The work has been supported by Innovative Economy Operational Program of National Ministry of Development in frames of the „Development and Production Implementation of „*Kruk*" Agricultural Aircraft Family", UDA_POIG.01.04.00-14-214/11-00.